Available online at www.sciencedirect.com

ScienceDirect

Procedia Structural Integrity 28 (2020) 208–217

Structural Integrity Procedia

www.elsevier.com/locate/procedia

1st Virtual European Conference on Fracture

Acoustic Emission NDT for monitoring hygro-mechanical reactions of coated pine wood: a methodological approach

Chiara Bertolin[a*], Lavinia de Ferri[a], Javad Razavi[a], Filippo Berto[a]

[a]*Norwegian University of Science and Technology, Department of Mechanical and Industrial Engineering, Richard Birkelands vei 2B, Trondheim -7491, Norway*

Abstract

Wood generally suffers drastic RH variations, strongly affecting its dimensional stability because of the gain or loss of adsorbed water. The proposed paper intends to investigate the applicability of a multi-technique approach for the estimation of crack length in softwood structures. The methodology foreseen the monitoring by acoustic emission (AE) of pine wood slices stressed in climate chamber inducing a strong RH variation from 80 to 30%, preceded by the sealing of the two radial surfaces with chemicals in order to force the loss of moisture only through the lateral surfaces. Samples obtained from the aged slices were submitted to fracture tests contemporary monitored by AE and a digital camera. Measurements of the crack length and overall amplitude of generated AE signals permitted the individuation of fit equations to be applied to AE data acquired during the aging at 30% RH allowing the reliable evaluation of the crack propagation extent in the slices. Furthermore, differences in the signals obtained by means of two different kind of AE sensors were evaluated in order to determine the main variables affecting data differences and create a methodology applicable to the interpretation of AE data collected on real structures affected by dimensional variations (swelling and /or shrinkage) due to important RH modifications.

* Corresponding author. Tel.:004748507716
E-mail address: chiara.bertolin@ntnu.no

2452-3216
10.1016/j.prostr.2020.10.026

Keywords: pine wood; acoustic emission; moisture diffusion; climate chamber, crack propagation.

1. Introduction

Wood is a widely diffused building material displaying a strong anisotropic structure leading its moisture-related dimensional changes to vary over its three principal anatomical axes.
Timbers can be usually realized using both softwood and hardwoods, having quite different cellular structures. Softwood in particular, is more widely used in Northern Europe and for this reason it represents the category investigated in this research. The softwood internal structure is quite easy being formed by basically two kinds of cells: tracheids, elongated cells providing both the structural support and the conducting pathways but without any living content, and parenchyma, not always present. These are axially elongated cells often containing compounds such as starch or resins. Additionally, bordered pits connecting tracheid permit the sap flow and the so-called resin canals laying in both radial and axial directions interconnecting each other. In softwood, radially cut surfaces can display a certain eccentricity with the pith shifted from its central position. This often occurs in leaning stems and branches and wood formed on the underside normally has different characteristics with respect to the upper one on the chemical, anatomical and physical points of view. It is called compression wood and it tends to develop a certain response to stress, being gravity the main acting force: rounded tracheids with thicker walls and intercellular spaces. Moreover, it shows an overall lower content in cellulose and consequently is higher in lignin (Butterfield, 2006).

As explained wood is a porous material that contains water, air and other substances and for this reason both weight and volume of wood, as well as other properties, are not constant: they can change when and if the material gains or loses moisture. Wood can contain both free and bound water, the first consisting in molecules absorbed in the cell lumens and intercellular spaces being vessels, pits, lumina and other voids in the wood anatomy (in the absorption phenomenon molecules are assimilated into the bulk of a solid or liquid). The latter is present as water molecules adsorbed within the cell walls (the adsorption is a surface process where molecules adhere to the surface of an adsorbent).

During wood drying it has been demonstrated that the loss of bound water begins before all liquid water is removed from the wood (Hernández & Cáceres, 2010; Passarini et al., 2015; Fredriksson & Thybring, 2019): as formulated by Almeida and Hernández (2006) this can be due to the fact that residual liquid water might be entrapped in cells creating the connections between lumina of adjacent cells (Hernández & Cáceres, 2010; Almeida & Hernández, 2006). Change in mechanical properties has been related to alterations in the relative proportions between bound and liquid water. As it has been reported, they can change when cell walls are in a non-saturated state and dimensional variations, eventually leading to failure being strictly related to modifications of the mechanical properties, can occur when capillary water is still present in the wood (Fredriksson & Thybring, 2019).

As a general rule, free water can be lost quite easily since the energy required is only slightly higher than that needed to evaporate from a flat surface, consequently, it can be maintained only at extremely high RH values (>99.9%). However, RH required to remove capillary free water is lower than 99.89% when the radius is smaller than 1 μm and can reach 89.77% when the radius is 0.01 μm (Fredriksson, 2019). On the other hand, water adsorbed is bound to the cell walls by means H-bonds (physical adsorption) and more energy (binding energy ~ 20 kJ/mol) is necessary to obtain the desorption and evaporation (Walker, 2006).

As anticipated, this reflects on the dimensional stability of wood, since shrinkage occurs as a consequence of modification of the RH conditions. Particularly, the overall volumetric shrink is proportional to the number of lost adsorbed water molecules but it does not occur at the same extend in the three directions, being wood an orthotropic material. The most affected direction is the tangential one, generally from 1.5 to 2.5 higher than the radial one (T/R ratio). On the other hand, the longitudinal shrinkage can be ignored, being extremely small (Spear and Walker, 2006).

Here the results obtained from experiments carried out coupling climate control and sample monitoring by means acoustic emission (AE) are proposed. The research aims to develop a method for the estimation of crack propagations in softwood such as pine due to changes in the environmental conditions. These stressful circumstances can, in fact, easily lead to damages in wooden structures, easily detectable using non-destructive techniques as AE. The following

mechanical tests of samples obtained by stressed pine slices permitted the calibration of the system and the extraction of transfer functions allowing the estimations of real cracks lengths.

2. Materials and Methods

Fully saturated slices of Scots pine wood (average thickness ~2 cm) have been acclimatized at 80% RH and constant temperature (20.5 °C) in the period 20/05/2019-07/06/2019 using an HPP-IPP^{plus} climate chamber (Memmert, Germany). The chamber is equipped with two lateral holes hermetically sealable to allow the passage of cables from the AE system used to monitor the pine slices for the whole period (see instruments details below). On 07/06/2019 the two radial surfaces of each slice were treated with sealing coatings and re-placed in climate chamber at the same temperature condition but dropping off the RH value to 30% for the subsequent period 07/06/2019- 28/06/2019. Also in this second part of the experiment, slices were constantly monitored by AE. Sealing the two radial surfaces it was expected to force moisture to be exchanged (lost) only through the lateral surfaces. Parallel, standard samples already shaped for the fracture tests (see below for samples shape details) were kept at RH= 50% for the whole duration of the test in order to provide a standard not-acclimatized reference.

2.1. The surface treatments

A 40% (w/v) solution of Paraloid B72 (Phase) in acetone (Sigma Aldrich) was prepared at 60°C in a closed container under magnetic stirring (80 rpm) in order to speed up the polymer dissolution. The Paraloid solution (P40) was deposited by brush on the wooden surfaces preliminary treated with a cellulose sand seal spray (Chestnut) commonly employed in the preparation of wooden materials in order to avoid water capillary rise. The spray was let to dry for 5 min before depositing the P40 solution (de Ferri et al., *in press*). Further tested materials were the Reinassence (R) microcrystalline wax, spread by means of a spatula, and tar deposited by brush. Tar treatments were performed in an external facility by professionals specialized in the preparation and deposition of such material. The choice of tar is related to its wide use as a protective material for wooden historical buildings, in particular medieval stave churches, being the research part of the activities of the SyMBoL (Sustainable Management of Heritage Buildings in a long-term perspective) Project.

Samples devoted to the realization of fracture tests were created from each pine slice immediately after the end of the acclimatization period at RH=30% performed in the climate chamber, i.e. on 28/06/2019. Samples' general shape is reported in Fig. 1, also showing some of the main measures except the length being this different for every sample. This was mainly due to the maximization of the number of samples obtained from each slice and to their eccentricity, being the pith shifted from the central position. After cut, every sample has been isolated and maintained in a separated plastic bag hermetically closed in order to avoid as much as possible variations in its moisture conditions. Fracture tests were performed in the following days.

2.2. Instrumental details

As already pointed out, all the samples were monitored by AE. In particular two systems were used at the same time on each slice: an AMSY-6 and an AMSY-4 (Vallen System GmbH, Icking, Germany). Consequently, on every slice a sensor connected to the first system and a sensor connected to the second one were attached. As concerning the AMSY-6 system, each AE channel was equipped with a VS900-M sensor (frequency operating range = 100–900 kHz) in line with an AEP5 signal preamplifier (2.5 kHz to 2.4 MHz). Each channel, sensor and preamplifier combination was kept fixed during all experiments.

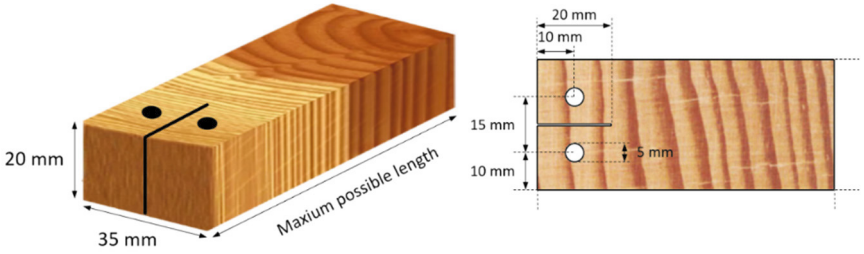

Figure 1: shape and dimensions of samples for fracture tests.

The rearm time and duration discrimination time were set to 3.2 and 1.6 ms, respectively, while pre- and post-trigger times were maintained equal to 0.2 and 0.4 ms, respectively. The signal sampling rate used to calculate the primary AE parameters was 10 MHz, whereas a value of 1 MHz was used to record the transient signal. Signals were acquired without applying any filter (bypass); then the first peak amplitudes (i.e., the maximum value of the first amplitude peak) were integrated to obtain the amplitude values to be verified in the attenuation models presented here. This approach, also used very recently by Zhang et al., 2019, effectively reduces the disturbances caused by the effects of reflection and refraction of AE waves on the results of amplitude attenuation.

Regarding the AMSY-4 system, each AE channel was equipped with a KRNBB-PC Glazer sensor with a "flat" frequency operating range between 10 kHz to 1 MHz in line with an AEP5 signal preamplifier (2.5 kHz to 2.4 MHz). Each channel, sensor and preamplifier combination was kept fixed during all experiments. The rearm time and duration discrimination time were both set to 0.4 ms. Similarly, the signal sampling rate used to calculate the primary AE parameters and to record the transient signal remained unchanged i.e. 10 MHz and 1 MHz respectively. Also with AMSY-4, the signal was acquired with bypass filter and the first peak amplitudes were integrated to further analysis.

In both cases, the disturbance caused by environmental noise was filtered using the system-predetermined threshold level set to 34 dB, plus a minimum system threshold of 6 dB based on the noise level (i.e., electronic and background noise) (ASTM E2374-16).

Fracture tests were carried out by means of a universal testing machine-UTM (MTS producer), securing the samples utilizing specially created grippers. Tests were performed at a displacement rate of 1.5 mm/min recording the stress/strain curves. Images from each test have been recorded by means of a F504B Stingray digital camera with a rate of 5 frames/s, synchronized with the UTM in order to individuate and analyze images corresponding to critical points in the stress/strain curve, getting the crack length value. Additionally, each test was also monitored by AE using the AMSY-4 system. The same combination of sensors, cables and amplifier used during the monitoring in climate chamber was kept for samples derived from corresponding slices (e.g. Sensors S1 and G1 were used on slice 1 and on samples for fracture test created from slice 1). For the standard reference samples sensors VS900-M S5 and S6 were used. The AE system, as well as the camera, were synchronized with the UTM during the acquisition. A resume of slices, treatments, sensors, samples code number, and dimensions is provided in Table 1.

3. Results and Discussion

As reported in section 2, AE signals have been recorded during both the stages of the experimental procedure occurred in the climate chamber and during the final experimental stage of the tensile tests for calibration purposes. As shown in Fig. 2, different patterns were obtained for the Vallen (V) and Glazer (G) sensors during the period at 80%RH. Fig. 2 reports exemplificative patterns obtained for V2 and G2 sensors and hypotheses have been formulated on the nature of such signals, whose distribution over time looks very different for the two typologies of employed sensors. In particular, the pattern observed for the V sensor (V2 in Fig. 2) seems to be compatible with the swelling of wooden structures due to the high RH conditions respect to the room conditions in which the wood was kept before the test.

Table 1: Details of pine wood slices, deposited treatments, used AE sensors (V=Vallen; G= Glazer), samples code number, and dimensions obtained from samples fracture tests.

Slice	Treatment	Sensors	Samples	Length (mm)
1	Microcrystalline wax	1V+1G	1.1	54
			1.2	64.2
			1.3	81.3
			1.4	50.5
2	Cellulose sand sealing spray + Paraloid 40%	2V+2G	2.1	63
			2.2	50
			2.3	78.5
3	Tar	3V+3G	3.1	63.2
			3.2	84
Standard	/	5V+6V	ST1	69.7
			ST2	47.3

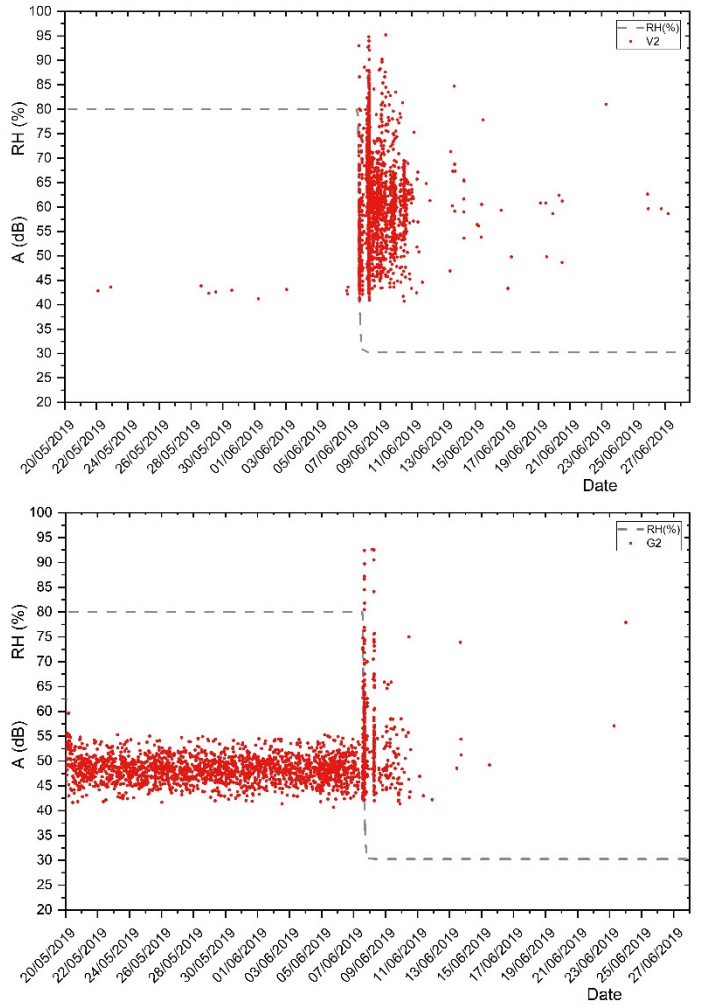

Figure 2: AE signals collected during the whole experiment by means of the Glazers (G2, left) and Vallen (V2, right) sensors on the pine wood slice treated with Paraloid and the cellulose sand sealing spray.

The AE activity was concentrated over the first days and successively, as the slice equilibrated with the environmental conditions into the chamber, it decreased. On the contrary, the G sensor (G2 in Fig. 2) showed a constant behavior during the whole period, probably more linked to noise caused by a progressive sensor detachment. In this work data elaborated from the Vallen sensors (V2) are more reliable as these sensors were easier to be fixed to both the slices' lateral surfaces during the exposition in the climate chamber and the specimens submitted to the fracture tests. In contrast, the Glazer sensors' geometry (longer and thinner than the Vallen ones) made their gluing to the surfaces more difficult and their detachment could occur easily due to their weight during both experimental stages (i.e. monitoring in the climate chamber and during the tensile tests).

In the experimental procedure, the sensors were removed and relocated just to apply the coating treatment on the slices before to change the RH conditions to 30%. The sensors (V2 and G2 in Fig. 2) detected many signals in the first days after the RH modification, and few on the long period. This is compatible with the occurrence of shrinkage movements of the wooden slices, whose extent is influenced by the deposited coatings acting as constrains.

The objective of this work is to demonstrate, that, through a correct calibration procedure – starting from the analysis of the AE detected energy emitted by the stressed material, it is possible to estimate the real macro crack length experimentally observed on a coated pine slice acclimatized in the climate chamber after a sudden RH change. The outcome of the data analysis reported in this work focuses, as an example, on the slice treated with Paraloid coupled to the sealing spray (slice 2) as this was one of the slices that – together with the tar-treated one - broke at the end of the acclimatization period at 30% RH. This is because this coating resulted excessively binding and did not allow the free movement of wood structures due to the induced loss of moisture.

Figure 3 shows all the steps of the data analysis done within the experimental procedure described in section 2 which saw the use of the climate chamber, UTM, AE and camera tools. Figure 3a reports the outcome of the tensile tests done with the UTM on the samples obtained from the acclimatized slice. From each tensile test, a set of critical points - constituted by a sequence of load increase stages and load drop stages – was obtained from the stress/strain curve. During load increase stages, a higher percentage of energy (i.e. approximatively 75% as reported in Pollock, 1970) is spent for mechano-chemical processes in plastic deformation of the wooden sample (e.g. for dislocation, nucleation and motion in the neighborhood of crack tip). This excess of released energy, being different from the elastic energy, cannot directly be related to the brittle crack propagation mechanism. At the opposite, during load decrease stages, the total energy is emitted rapidly for making the crack progressing suddenly (and not steadily). This makes the majority of the released energy coinciding with the elastic energy detected by the acoustic emission system. This brittle mechanism of fracture is the most interesting for the AE calibration purposes. The second stage in data analysis (Figure 3b) concerns the crack length estimation for each of these critical load increase and decrease points.: it has been obtained from the analysis of images acquired by the camera during the splitting of the samples. Then the sum of the AE energy recorded during stages of load increase and decrease have been analyzed separately for each sensor as a function of the crack length propagation (Figure 3c for load increase and 3d for load decrease stages).

For the 3 specimens obtained by the pine slice 2 the obtained fit equations relating AE energy (E_{AE}) with the crack length (l_c) are reported in Table 2, except for G2 on S2.1 where no enough points were collected.

Table 2: Calibration curves equations obtained from samples cut from slice 2.

Sample	Sensor	State	Best fit equation	R^2
S2.1	V2	Slow crack propagation	$l_c = -1.03 + 2.23 \cdot 10^{-7} \cdot E_{AE}$	0.91
		Fast crack propagation	$l_c = -46.50 + 4.56 \cdot 10^{-6} \cdot E_{AE}$	0.79
S2.2	V2	Slow crack propagation	$l_c = 2.14 + 1.60 \cdot 10^{-6} \cdot E_{AE}$	0.87
		Fast crack propagation	$l_c = 2.52 + 5.06 \cdot 10^{-6} \cdot E_{AE}$	0.99
	G2	Slow crack propagation	$l_c = 3.56 + 3.36 \cdot 10^{-6} \cdot E_{AE}$	0.99
		Fast crack propagation	$l_c = 0.38 + 4.50 \cdot 10^{-7} \cdot E_{AE}$	0.97
S2.3	V2	Slow crack propagation	$l_c = -0.2 + 1.00 \cdot 10^{-7} \cdot E_{AE}$	0.98
		Fast crack propagation	$l_c = 0.024 + 1.33 \cdot 10^{-7} \cdot E_{AE}$	0.99
	G2	Slow crack propagation	$l_c = -0.46 + 1.97 \cdot 10^{-7} \cdot E_{AE}$	0.99
		Fast crack propagation	$l_c = 0.02 + 3.15 \cdot 10^{-7} \cdot E_{AE}$	0.99

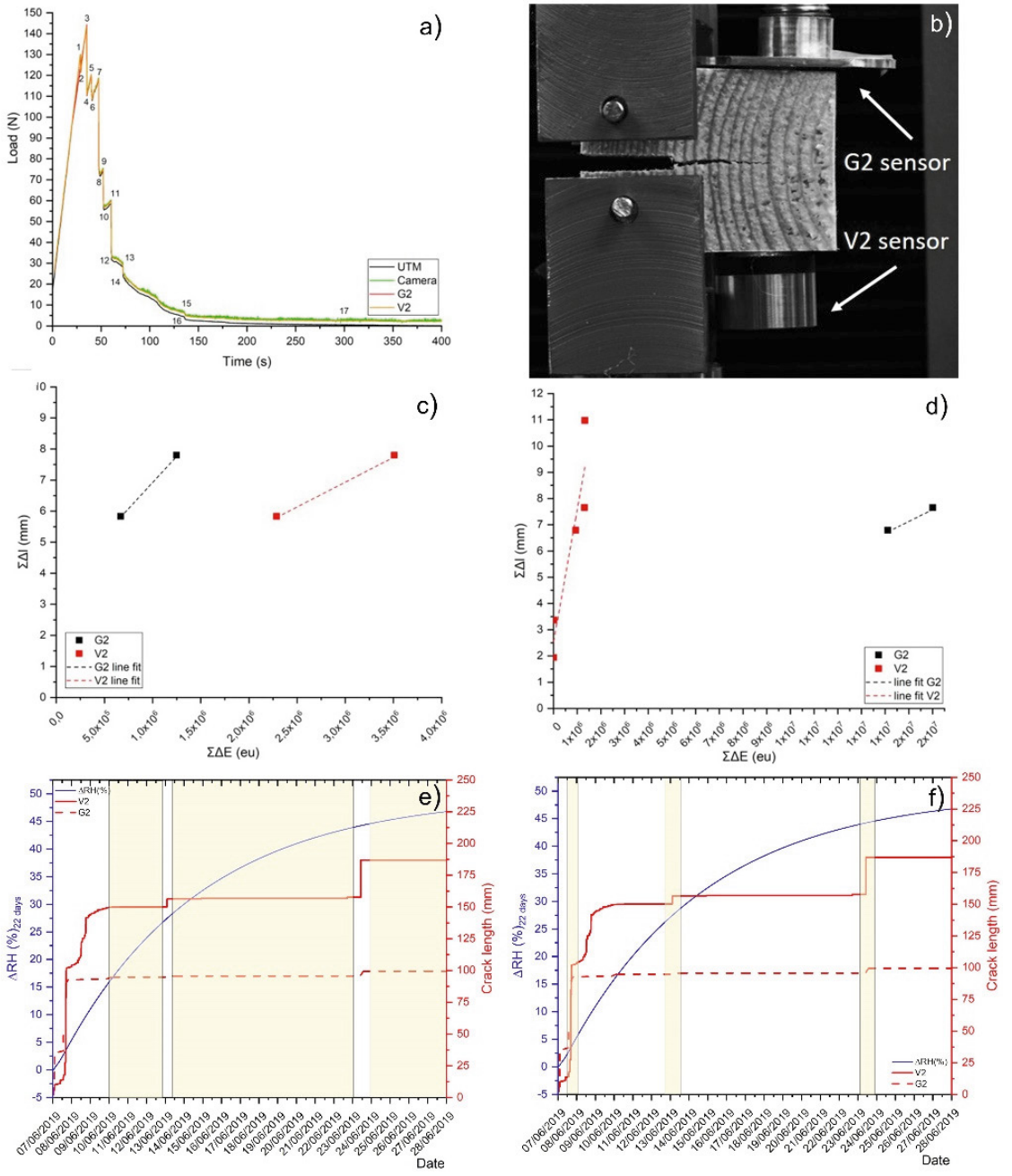

Figure 3: a) example of a Time (s)/Load (N) curve obtained for the three instruments acquiring simultaneously (UTM, camera and AE) with stages of load decrease and increase; b) example of a sample during the fracture test coupled to the AE system through the two types of sensor (G Glaser and V Vallen). Image used for the measurement of the crack length; c) and d) Best fit of AE data acquired during the fracture test (ΣΔE versus ΣΔl or crack length) for the two Glaser (G) and Vallen (V) sensors during load increase and decrease stages respectively; d) and e) crack length propagation estimated applying the best fit equations to AE data acquired in the climate chamber on the Paraloid and cellulose seal spray slice for load increase and decrease stage respectively.

The stages reported in Figure 3 are part of the calibration procedure which can be applied to AE energy data acquired during in situ monitoring to estimate the mechanical decay appearance (i.e. macro crack) which naturally may propagate under climate load conditions. In the case of our experimental procedure, this long-term monitoring procedure was carried out on the treated pine slice acclimatized in the climate chamber. The application of the proposed method for the elaboration of AE and fracture data observed in the climate chamber resulted able to distinguish between a short crack length occurred during stages of ductile fracture mechanisms at micro level (see slow propagation rate zones highlighted in yellow in Figure 3e) and long crack length occurred during stages of load decrease (fast crack propagation zones highlighted in yellow in Figure 3f), indicative of brittle fracture mechanism at macro level. As already pointed out, these stages are the only which can explain, with the help of the AE NDT, the macro fracture visible experimentally.

The total calculated crack of *ca*. 130 mm length, resulting from the three events of brittle fracture reported in Figure 3e appears, in fact, to be in accordance with the experimental evidence of the final macro damage that was measured in a 90 mm length linear fracture. The discrepancy is an intrinsic defect of the AE monitoring technique that cannot be eliminated. It is caused by the spurious energy estimated in 25% of the total detected energy that is not elastic and that cannot be directly connected with acoustic emissions (Pollock, 1970). In the case of our example, this additional energy brings to an overestimation of 40 mm in the crack length.

Figure 4 compares the results obtained from the application of the calibration procedure on the monitored AE data for slice 2, treated with the Paraloid and cellulose sand sealing spray and cracked at macro level, with those attained for slice 1, treated with microcrystalline wax and uncracked. In the case of slice 1, the fracture elongation estimated by the calculations results lower than 2 mm in accordance with the visual inspection of the slice which after the acclimatization period resulted unharmed, thus demonstrating the reliability of the method.

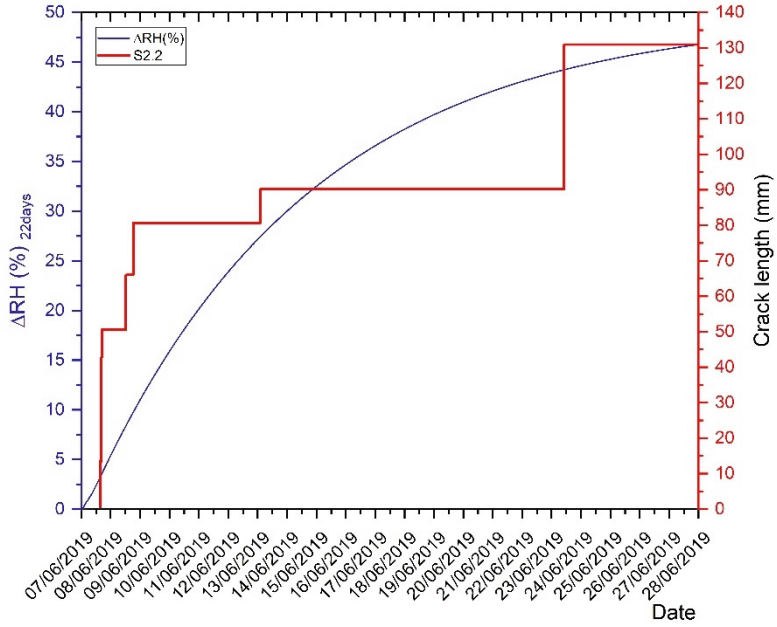

Figure 4: Crack propagation as a function of the RH change occurred in the climate chamber as obtained from AE monitored data acquired by means of a Vallen sensor. Blue line: RH values in the chamber. Red line: crack length propagation in mm for the pine slice treated with Paraloid and the sealing spray that showed macro damage. Back full, dashed and dotted lines: crack length propagation < 2mm on pine sample treated with microcrystalline which did not show decay.

Last but not least, in Figure 4 the damage progression (i.e. the crack length in millimeters) is associated with the cause of the decay that is the climate load reported in terms of RH variation within the pine slice. This ΔRH is equaled to the equilibrium value reached by the slice after the first stage of the acclimatization period (i.e. 80% RH) minus the actual RH value calculated using a response time of 22 days (see blue line in Figure 4). The plot highlights as more than half of the crack propagation at macro level occur within the first 41 hours after the change, being the slice subjected to a ΔRH of 10% with a rate of 0.25% RH/h. On the other hand, the rest of the decay occurs in two additional stages: the first after 6 days from the change when the ΔRH suffered by the slice arrived to 27.5%, and the last after more than 16 days when the slice arrived to a ΔRH of ca 44%.

4. Conclusions

Three different sealing treatments were deposited on the radial surfaces of pine wood slices after an acclimatization period of 21 days in climate chamber at 80% RH. An abrupt RH variation has been induced dropping off the value to 30% and maintaining the treated slices at these conditions for the following 18 days. A method to predict the extent of the eventual crack formation and propagation in the wooden slices has been developed starting from the monitoring of the slices by means of acoustic emission during the whole "acclimatized" period and performing fracture tests on samples obtained from the corresponding pine slices. AE and crack length data obtained during the tensile tests permitted to derive a set of points with load increase and decrease stages representative respectively of energy spent to deform plastically the wood at micro level and to cause brittle fracture at macro scale. Specifically, only the load decrease stages can be used in the calibration process of AE data as they are linearly related to the emitted elastic energy during fracture. The transfer function during these events only can be used to transform the AE energy data acquired during the period in which the slices were kept at 30% RH to assess the effect of the climate load. In this way, a reliable evaluation of the crack propagation extent in the slice positioned in the chamber was obtained and differences within the calculated and observed crack extension were underlined. The tested methodology looks promising as it was able to predict both the observed macro and micro damages on different pine coated slices. The obtained results were comparable, within the limitation of the technique, with the experimental evidence highlighting as the proposed method of AE data analysis offers early warning information in assessing mechanical decay of wood coated material subjected to climate changes.

Acknowledgments

The research activity has been realized in the frame of the "SyMBoL – Sustainable Management of Heritage Building in a Long-term Perspective" Project (Project No. 274749) founded by the Norwegian Research Council.

References

Almeida G., Hernández R.E., 2006. Changes in Physical Properties of Yellow Birch Below and Above the Fiber Saturation Point. Wood and Fiber Science 38, 74-83.

Butterfield B., 2006. The Structure of Wood: Form and Function, in "*Primary Wood Processing Principles and Practice*", 2nd edition. In: Walker J. F. (Ed). Springer. pp. 1-20.

Hernández R.E., Cáceres C. B., 2010. Magnetic resonance microimaging of liquid water distribution in sugar maple wood below fiber saturation point. Wood and Fiber Science 42, 259-272.

de Ferri L., Strojecki M., Bertolin C., Preliminary results on surface treatments on wood, IOP Conf. Series: Materials Science and Engineering, *in press.*

Fredriksson M., 2019. On Wood–Water Interactions in the Over-Hygroscopic Moisture Range-Mechanisms, Methods, and Influence of Wood Modification. Forests 10, 779.

Fredriksson M., Thybring E. E., 2019. On sorption hysteresis in wood: Separating hysteresis in cell wall water and capillary water in the full moisture range. PLOS ONE E 14(11), e0225111

Passarini L., Malveau C., Hernández R. E., 2015. Distribution of the equilibrium moisture content in four hardwoods below fiber saturation point with magnetic resonance microimaging. Wood Science and Technology 49, 1251-1268.

Spear M., Walker J., 2006. Dimensional instability in Timber, in "*Primary Wood Processing Principles and Practice*", 2nd edition. In: Walker J. F. (Ed). Springer. pp. 95-120

Walker J., 2006. Water in wood, in "*Primary Wood Processing Principles and Practice*", 2nd edition. In: Walker J. F. (Ed). Springer. pp. 69-94.

Zhang J., Yang S., Hao R., Gu X., 2019. Amplitude attenuation laws of acoustic emission waves in plate structures, Tecnología e ingeniería mecánicas, 94, 67–74.

Pollock, A.A. 1970. Acoustic Emission from solids undergoing deformation. PhD thesis. University of London